Langmuir

Article

pubs.acs.org/Langmuir

Mapping the Mechanical Properties of Cholesterol-Containing Supported Lipid Bilayers with Nanoscale Spatial Resolution

Nicole Shamitko-Klingensmith,[†,‡] Kelley M. Molchanoff,[‡] Kathleen A. Burke,[†] George J. Magnone,[†] and Justin Legleiter*[,†,‡,§]

[†]The C. Eugene Bennett Department of Chemistry, [‡]WVnano SAFE, and [§]the Center for Neurosciences, West Virginia University, Morgantown, West Virginia 26505, United States

Supporting Information

ABSTRACT: It has been demonstrated that many biological processes are influenced by mechanical changes in membranes comprised of a variety of lipid components. As a result, the ability to map physicomechanical properties of surfaces with high temporal and spatial resolution is desirable. Tapping mode atomic force microscopy (AFM) has proven to be a useful technique for imaging biological surfaces due to its ability to operate in solution; however, access to information concerning the mechanical properties of these surfaces can also be obtained by reconstructing the time-resolved tip/sample force interactions during the imaging process. An advantage of such an approach is the direct correlation of topographical features with mechanical properties. Reconstruction of the tip/sample force is achievable by a technique called scanning probe acceleration microscopy (SPAM), which treats the cantilever as an accelerometer. The acceleration, which is directly related to the tip/sample force, of the cantilever is obtained by taking the second derivative of the cantilever deflection signal during a tapping mode AFM experiment in solution with standard cantilevers. Herein, we describe the applicability of SPAM to study mechanical properties of supported lipid bilayers with nanoscale spatial resolution via numerical simulations and experiment. The maximum and minimum tapping forces respond to changes in specific surface mechanical properties. Furthermore, we demonstrate how these changes can be used to map relative changes in the Young's modulus and adhesive properties of supported total brain lipid extract bilayers containing exogenous cholesterol. Finally, the ability of SPAM to distinguish nanoscale lipid raft domains based on changes in local mechanical properties is demonstrated.

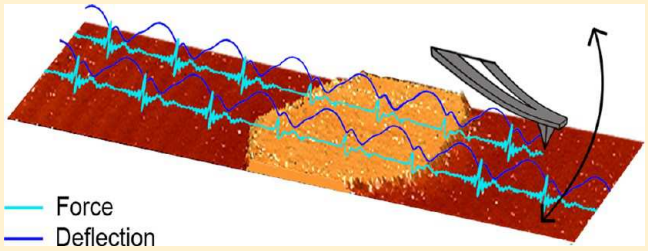

INTRODUCTION

Of particular interest are technologies to quantitatively and temporally monitor, track, and/or characterize mechanical properties of biologically relevant surfaces with nanoscale spatial resolution.[1] In particular, there is a need to further develop technologies in scanning probe microscopy that are capable of simultaneously tracking morphology and mechanical surface properties in a noninvasive manner under physiologically relevant conditions. A potential advantage of such technologies is the ability to directly correlate surface topography with mechanical properties with nanometer spatial resolution. A promising technology in this regard is scanning probe acceleration microscopy (SPAM),[2] which is based on tapping mode atomic force microscopy (AFM). Tapping mode AFM, a widely used dynamic imaging technique, maps surface topographies by systematically monitoring the oscillation amplitude of a cantilever affixed with an ultrasharp tip probe that physically interacts with the surface.[3,4] In this imaging mode, the cantilever is commonly driven near its resonance frequency ω by means of a bimorph element near its base. Intermittent tip/sample contact causes the cantilever oscillation amplitude to decrease from the "free" amplitude A_0 to a tapping amplitude A, as the sample surface is a repulsive barrier that limits the oscillation amplitude of the cantilever. For rigid surfaces, the oscillation amplitude of the cantilever decreases linearly as a function of the separation distance between the tip and the sample D_0. As a result, the surface topography can be determined by raster scanning the tip in the xy plane across the surface and implementing a feedback loop that continuously corrects the vertical (z) extension of the piezoelectric scanner to maintain a constant set-point ratio, $s = A/A_0$. SPAM reconstructs the time-resolved tip/sample force during each individual tapping event in a tapping mode AFM experiment in solution. These tapping events contain information related to the mechanical properties of the surface such as Young's modulus and adhesion. The underlying principle behind SPAM is that in tapping mode AFM the cantilever acts as an accelerometer from which the tip/sample forces can be extracted during regular operation.[2] This method utilizes the second derivative of the deflection signal to recover the tip acceleration trajectory. As SPAM can be applied in solution, it has potential to probe biologically relevant surfaces, such as supported bilayers, cells, and other biological surfaces under the influence of external factors.

Received: July 5, 2012
Revised: August 22, 2012
Published: August 27, 2012

The first method to extract time-resolved tip/sample forces during regular tapping mode AFM imaging was reported by Stark et al., who accomplished this by taking the inverse Fourier transform of the Fourier-transformed cantilever trajectory divided by its transfer function.[5] Since then, several methods have been developed to reconstruct the time-resolved tip/sample forces.[2,6−14] These approaches, including SPAM, present several experimental advantages over other traditional AFM techniques. As they are based in the tapping mode, these methods maintain the high spatial resolution associated with tapping mode imaging and are relatively nondestructive, which is important when imaging fragile biological samples. Other methods that measure mechanical properties of surfaces (i.e., force volume imaging and nanoindentation) can require large deformation of soft samples, leading to decreased spatial resolution and possibly damaging the surface, whereas tapping mode forces are adaptive to changes in surfaces properties. Furthermore, reconstructing tapping forces allows for mapping surface properties at scan rates used for simple tapping mode AFM imaging, which are typically much faster than other methods, as images can be captured in minutes. Finally, as the cantilever is typically oscillated at a frequency in the range of 8−10 kHz in tapping mode AFM in solution, the forces associated with thousands of individual tip/sample tapping events can be measured every second.

A particularly important application of using time-resolved tip/sample forces is mapping the mechanical properties of supported lipid bilayers, which can be used as models of cellular membranes. Membranes are vital components of all living systems with many biochemical reactions occurring on these surfaces. Cell membranes are two-dimensional liquid-crystalline structures comprised of fluid assemblies of amphiphilic molecules.[15−17] Biological membranes are typically comprised of a large, diverse mixture of lipid components, and this composition plays a necessary role in membrane structure and function. To function properly, biological membranes require high lateral fluidity while retaining structural integrity. As physical entities, the physical properties of biological membranes must enable them to perform a variety of functions properly and withstand mechanical and chemical stresses in their physiological environment. Because of the immense complexity of biological membranes, model membranes, consisting of a variety of lipid components, have played an integral part in understanding membrane function and physical properties.[1,18−20] Alterations in lipid organization can profoundly affect many cellular functions, including signal transduction and membrane trafficking.[21,22] One of the major components of lipid membranes is cholesterol. Cholesterol is an important regulator of lipid organization, and sophisticated mechanisms are employed to maintain cholesterol levels in membranes *in vivo*.[23] The failure of these control mechanisms are associated with a variety of diseases, such as atherosclerosis.[24] Cholesterol has pronounced effects on the mechanical and physical properties of lipid bilayers, including molecular fluidity,[25,26] compressibility,[27] stiffness,[28] resistance to shear stress,[15] and thickness.[20,29] As a result, cholesterol plays a vital role in regulating the biophysical/mechanical properties of membranes, with pronounced consequences for cell physiology.

Here, supported total brain lipid extract (TBLE) bilayers with the addition of varying amounts of exogenous cholesterol were used as a model system to demonstrate how time-resolved tip/sample tapping forces can be used to understand some physical properties of supported lipid bilayers. TBLE is comprised of a complex mixture of physiologically relevant membrane components, i.e., acidic and neutral phospholipids, gangliosides, cholesterol, sphingolipids, and isoprenoids (Figure 1), increasing its applicability as a model system. For example, brain lipid extract has been used as a model surface in studying the interaction of amyloid proteins with membranes[26,30,31] and as a mimic of the blood brain barrier.[32] Numerical simulations of a complete tapping mode AFM experiment are presented to demonstrate how specific features of tip/sample tapping forces change in response to the material properties of a surface. These simulations aid in the interpretation of experimental data obtained on the TBLE/cholesterol supported bilayer systems. The dependence of the tip/sample tapping forces on the set-point ratio is briefly presented, as understanding this relationship is critical in successfully comparing results between experiments. SPAM experiments on a variety of supported TBLE/cholesterol bilayer systems are presented, providing insights into the local compressibility of the supported bilayer perpendicular to the plane of the surface and the adhesion of the supported bilayer with respect to the AFM tip. Finally, a supported TBLE bilayer with 30% exogenous cholesterol was heated, resulting in the formation of lipid raft domains, which was used to demonstrate the lateral resolution of mapping relative mechanical properties of supported bilayers with SPAM.

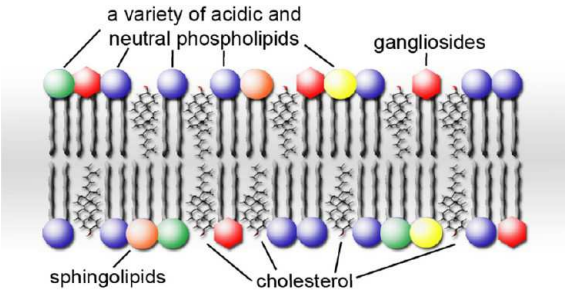

Figure 1. Schematic of a total brain lipid extract (TBLE) bilayer. Supported TBLE bilayers are comprised of a physiologically relevant ratio of membrane components, i.e., acidic and neutral phospholipids, gangliosides, cholesterol, sphingolipids, and isoprenoids. In these studies, exogenous cholesterol was added to the supported TBLE bilayer system.

MATERIALS AND METHODS

Numerical Simulations. Tapping mode AFM experiments in solution were simulated using MATLAB and SIMULINK (Math Works Inc. Natick, MA). The SIMULINK model is shown in Supporting Information Figure 1. In these simulations, the cantilever was modeled as a single degree of freedom damped driven harmonic oscillator[33−36]

$$m_{\text{eff}}\ddot{z} + b\dot{z} + k[z - D_0 + a_0 \sin(\omega t)] = F_{\text{ext}} \quad (1)$$

where m_{eff} is the effective mass of a cantilever, b is the damping coefficient, k is the cantilever spring constant, a_0 is the drive amplitude, ω is the drive frequency, D_0 is the resting position of the cantilever base, F_{ext} is the tip/sample force, and z is the position of the cantilever with respect to the surface (Supporting Information Figure 1). The second mode of the cantilever deflection can play a significant role in cantilever motion near surfaces in fluids;[37] however, such contributions from the second mode are negligible when imaging soft biological samples in solution.[38] While imaging in the tapping mode, the separation distance between the cantilever and surface is continually changing due to the oscillation of the cantilever. The tip

dx.doi.org/10.1021/la302705f | *Langmuir* 2012, 28, 13411−13422

is also allowed to intermittently strike the surface once during each oscillation cycle. As a result, there are two tip/sample interaction regimes: (1) when the tip and surface are not in contact and (2) when the tip and surface are in contact during the tapping event when the separation distance z is smaller than the interatomic distance (a_{DMT}). A tip near a surface in solution experiences van der Waals forces and electric double layer forces, which can be described by the Derjaguin–Landau–Verway–Overbeek (DLVO) theory;[39] however, the forces associated with the electric double layer effect are negligible under high salt concentration, which results in a relatively short Debye length.[38] As experiments described later were performed under a high salt condition (PBS buffer), the external force can be approximate and simplified using the van der Waals interaction between a sphere and flat surface[39]

$$F_{ext} = -\frac{HR_{tip}}{6z^2} \quad \text{for } z > a_{DMT} \tag{2}$$

where H is the Hamaker constant and R_{tip} is the tip radius.[40] During the second interaction regime where the probe tip contacts the surface, the tip/sample force is described by a DMT potential (Derjaguin–Muller–Toporov)

$$F_{ext} = \frac{4}{3\pi\kappa_{eff}}\sqrt{R}(a_{DMT} - z)^{3/2} - \frac{HR_{tip}}{6a_{DMT}^2} \quad \text{for } z \le a_{DMT} \tag{3}$$

with

$$\kappa_{eff} = \frac{1 - \upsilon_{tip}^2}{\pi E_{tip}} + \frac{1 - \upsilon_{sample}^2}{\pi E_{sample}} \tag{4}$$

where E_{tip}, ν_{tip} and E_{sample}, ν_{sample} are respectively the Young's modulus and Poisson coefficient of the tip and the sample.

The cantilever deflection signal, rather than the position (z), is actually monitored in real AFM systems. While the position and deflection signal differ minimally for systems characterized by low damping (high values of Q), these signals differ drastically in a highly damped (or low Q) systems such as those associated with fluid tapping mode AFM.[37,41,42] The deflection signal (y) is related to position by

$$y = z - D_0 + a_0 \sin(\omega t) \tag{5}$$

A feedback loop equipped with an integral gain was incorporated into the model to allow for the complete simulation of the scanning process in tapping mode AFM (Supporting Information Figure 1). This feedback loop was implemented by determining the cantilever oscillation amplitude for each cycle, comparing it to a specified set point amplitude, and adjusting the cantilever position with respect to the surface to maintain the set point amplitude. Model surface topographies were used that consisted of a 5 nm step. The ability to change the values of the Hamaker constant and surface Young's modulus during the simulation was implemented, and this was coordinated with changes in the model surface topography.

Sample Preparation. Total brain lipid extract (TBLE) (Avanti Polar Lipids) and cholesterol were dissolved in chloroform (ACROS Organics) and mixed at appropriate ratios based on mass percentage. The chloroform was removed using a Vacufuge (Eppendorf). The resulting lipid films were resuspended in phosphate buffered saline (PBS) (pH 7.3) at a concentration of 1 mg/mL. By using liquid nitrogen, bilayers and multilayer lipid sheets were formed by five sequential freeze–thaw cycles. The lipid suspensions were then sonicated for 30 min at 40 °C to promote vesicle formation. The suspended vesicle solution was diluted 20 times, and 35 μL was injected directly into the AFM fluid cell onto a freshly cleaved mica surface. Over time, small, supported bilayer patches formed on the mica surface. The relative concentrations of different components in TBLE and solvents of extractions are available from the Avanti Polar Lipids Web site.

AFM Imaging Conditions. *In situ* AFM experiments were performed with a Nanoscope V Multimode scanning probe microscope (Veeco, Santa Barbara, CA) equipped with a tapping fluid cell and a V-shaped oxide-sharpened silicon nitride cantilever with an advertised spring constant of 0.27 N/m (Budget Sensors). While 0.27 N/m was the average spring constant of the cantilevers provided by the manufacturer, the individual cantilevers used in this study had spring contants ranging from 0.4 to 0.5 N/m when calibrated in our lab. Images were acquired with the use of a closed-loop "vertical engage" J-scanner. Scan rates were set at 1.95 Hz with cantilever drive frequencies ranging from approximately 8 to 9 kHz. Images were captured at 5 × 1.25 μm and 512 × 128 pixel resolutions. The temperature was controlled using the Bio-Heater accessory for the multimode AFM (Veeco, Santa Barbara, CA) and monitored with a thermister incorporated into the fluid cell.

Scanning Probe Acceleration Microscopy (SPAM). SPAM analysis was used to reconstruct every tapping event during AFM imaging as described.[2] Briefly, cantilever deflection trajectories were simultaneously captured during imaging through an AFM signal access module (Veeco) by using a CompuScope 14-Bit A/D Octopus data acquisition card (Gage Applied Technologies, Lachine, QB, Canada) and custom-written software. Trajectories were captured at 2–5 MS/s and 14-bit resolution with a resolution of 1–2 V. The trajectory of the cantilever was filtered using a Fourier transform based harmonic comb filter. In this process only intensities corresponding to integer harmonic frequencies are kept, and these are used to reconstruct a deflection signal, $y_{rec}(t)$, by inverse Fourier transform based on the equation

$$y_{rec}(t) = \hat{f}^{-1}\left[y(\omega)\sum_{k=1}^{N}\delta(\omega - k\omega_{oper})\right] \tag{6}$$

where ω_{oper} is the operating frequency and δ is the Dirac's delta function. The summation is carried out up to N, which is the highest harmonic still distinguishable above the noise level. N was typically 20–25 in these experiments. Once $y_{rec}(t)$ is obtained, the second derivative of the cantilever trajectory is taken and multiplied by the effective mass, m_{eff}, of the cantilever to obtain the time-resolved tapping force between the tip and sample based on substituting eq 5 into eq 1 and rearranging to obtain

$$\ddot{y} = \frac{1}{m_{eff}}[F_{ext} - b\dot{y} - ky - m_{eff}\omega^2 a_0 \sin(\omega t) + ba_0\omega\cos(\omega t)] \tag{7}$$

The SPAM analysis was not performed in real time; rather, the tapping forces were reconstructed from digitized cantilever deflection trajectories after the image was captured.

Using a thermal tuning method,[43] the spring constant and resonance frequency were obtained for the determination of m_{eff} by the equation

$$m_{eff} = \frac{k}{\omega^2} \tag{8}$$

This was done by measuring cantilever displacement in response to thermal noise in a frequency domain near the cantilevers resonance frequency. The area under the resonance peak, fit with a Lorentzian function, is related to the power of the cantilever displacement, and from this information the spring constant can be determined by the equation

$$k = \frac{k_B T}{P} \tag{9}$$

where k_B is the Boltzmann constant, T is the temperature, and P is the area of the power spectrum due to thermal noise. The acquired m_{eff} was used to convert the tip acceleration into units of force.

RESULTS AND DISCUSSION

Numerical Simulations Demonstrate That Time-Resolved Tip/Sample Force Changes in Response to Surface Mechanical Properties. To understand changes of the time-resolved tip/sample force interaction in response to

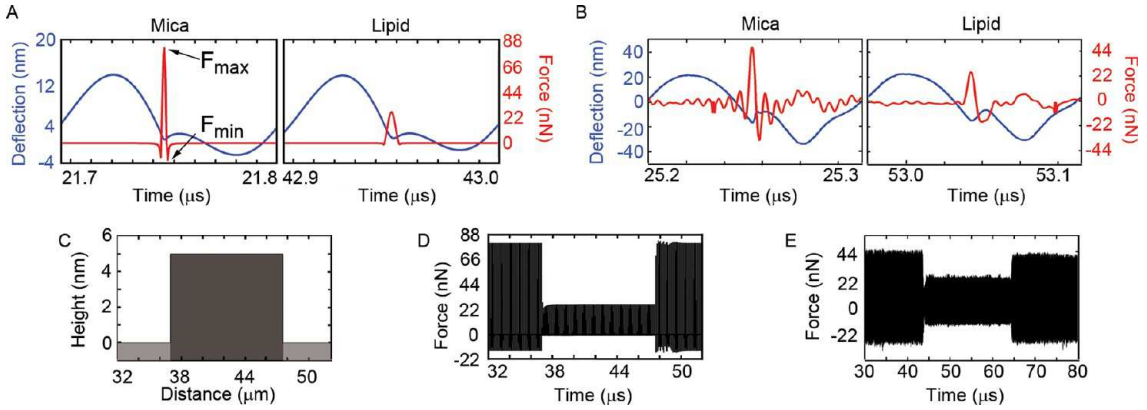

Figure 2. Simulations of the tip/sample force interaction associated with imaging a single scan line capture features of experiment. (A) Simulations of the cantilever deflection trajectory (blue) and tip/sample force interaction (red) are comparable to (B) experiment. F_{max} and F_{min} are indicated for both the simulation and experiment. To simulate the imaging process, a (C) model surface was constructed that contained a 5 nm step, which resembles our experimental supported bilayer patch/mica system. The Young's modulus and Hamaker constant on the step could be altered with respect to the regions before and after the step. Before and after the step, E = 60 GPa and H = 3.5 aJ. (D) Simulated force trajectories corresponding to imaging the entire model surface (the 5 nm step had E = 20 GPA and H = 0.35 aJ for the presented example) are comparable to (E) experimental reconstructed force trajectories taken from a single scan line in which a bilayer patch on mica was imaged (exposed mica before and after the supported bilayer patch).

mechanical properties of surfaces, numerical simulations of the entire fluid TMAFM imaging process were performed on predetermined surface morphologies. The effect of changing the sample Young's modulus on the imaging process was explored using eqs 3 and 4. Changes in the adhesive forces between the tip and surface were modeled by adjusting the Hamaker constant in eqs 2 and 3 because the Hamaker constant is related to the surface free energy (γ) between two materials by[39]

$$\gamma = \frac{H}{24\pi a_{DMT}} \approx \frac{H}{2.1 \times 10^{-21}} \quad (10)$$

Changes in Young's modulus and the Hamaker constant were synchronized with the predetermined surface topography to simulate the imaging process on a wide array of scenarios. For the simulations performed here, the model surface topography consisted of a 5 nm plateau with varying physical properties (Hamaker constant and Young's modulus). Simulations were performed with typical experimental parameters and properties of commercially available silicon nitride cantilevers that were used in experiments. These parameters and cantilever properties were drive frequency of 8−10 kHz, spring constant of 0.5 N/m (this value was chosen to match the measured spring constants of cantilevers used in the experimental portion of this study), free amplitude of 25 nm, and a set point ratio of 0.7 (tapping amplitude of 17.5 nm). Simulation scan parameters were chosen to correspond to imaging a 2 μm line with a scan rate of 2 Hz.

To verify the ability of the model to capture features associated with operating tapping mode AFM in fluids, simulated deflection trajectories and time-resolved tip/sample forces for a single oscillation cycle were compared to those obtained from experiment (Figure 2A,B). For this comparison, values of the Young's modulus and Hamaker constant were set to simulate imaging either a mica or supported lipid bilayer surface. The model captured the characteristic anharmonic deflection trajectory associated with tapping mode AFM.[41] The simulated time-resolved tip/sample force interaction also corresponded well with those obtained from real AFM experiments, as recovered by the SPAM technique. There are two main features of the time-resolved tip/sample force that were used in this study: (1) the maximum tapping force (F_{max}) per oscillation cycle (defined as the peak or largest positive force experienced between the tip and surface (as indicated in Figure 2A) and (2) the minimum tapping force (F_{min}) per oscillation cycle (defined as the minimum or largest negative force experienced between the tip and surface also indicated in Figure 2A). To further validate the model, simulations were performed of imaging a model surface (Figure 2C) on which the Young's modulus and Hamaker constant were changed on the step portion to approximate a lipid bilayer supported on a mica surface. The dynamic changes of the simulated time-resolved tip/sample force trajectory of the entire scan line captured the features observed in the tip/sample forces associated with imaging a supported lipid bilayer on mica obtained from experiment (compare Figures 2D and 2E). Such features included a reduced F_{max} and F_{min} associated with the tip/sample force when imaging the model step in simulation or the supported lipid bilayer in experiment.

With a working model of in solution tapping mode AFM, simulations aimed at determining the effect of altering the mechanical properties of surfaces on the measured topography and time-resolved tip/sample force interaction were performed (Figure 3). For these simulations, the Young's modulus was 60 GPa before and after step, and the Hamaker constant was 3.5 aJ. The true height of the model step was 5 nm. The Young's modulus on the step region of the model surface was systematically altered in a series of simulations while keeping the Hamaker constant at 0.35 aJ and all other imaging parameters constant (Figure 3A−D). As the step became more compliant to compression (smaller value of Young's modulus), the simulated measured height of the step decreased and was always smaller than the true 5 nm height (Figure 3A). The increased compliance of the step resulted in the tip pushing further into the surface and a longer contact time between the tip and surface (Figure 3B). While changes in the Young's modulus did not alter the magnitude of F_{min} between the tip and surface, F_{max} increased with larger values of Young's modulus (Figure 3C), as a result of the κ_{eff} term in eq 3. As tapping mode AFM images surfaces by maintaining the total

dx.doi.org/10.1021/la302705f | Langmuir 2012, 28, 13411−13422

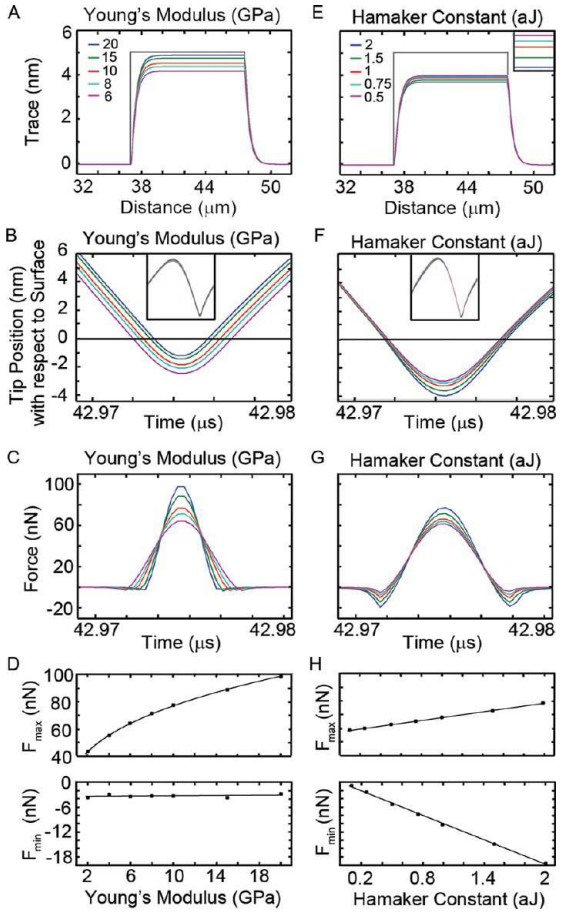

Figure 3. Simulations demonstrating the role of the Young's modulus and Hamaker constant on the measured topography and tip/sample interaction forces. The column of plots on the left present results for simulations that varied the Young's modulus with a constant Hamaker constant: (A) the measured topography of a soft step on a hard substrate, (B) the position of the cantilever with respect to the sample surface during a tapping event, (C) the tip/sample force associated with a tapping event, and (D) F_{max} and F_{min} plotted as a function of Young's modulus. The column of plots on the right present results for simulations that varied the Hamaker constant with a constant Young's modulus: (E) the measured topography of a soft step on a hard substrate, (F) the position of the cantilever with respect to the sample surface during a tapping event, (G) the tip/sample force associated with a tapping event, and (H) F_{max} and F_{min} plotted as a function of the Hamaker constant. The changes in Young's modulus and Hamaker constant were made only on the 5 nm step of the model surface (as shown in part C).

force per oscillation cycle (accomplished by maintaining the set-point amplitude), the larger F_{max} associated with imaging the more rigid surface was compensated for by the shorter contact time between the tip and surface. As a result, only the magnitude of the F_{max} increases with larger values of Young's modulus while F_{min} is unresponsive to changes in the Young's modulus (Figure 3D). The relationship between F_{max} and Young's modulus can be described by a power law.

The impact of changing the surface free energy between the tip and surface on the time-resolved tip/sample force was explored by simulations performed with variations in the value of the Hamaker constant (based on eq 6) on the step region of the model surface while keeping the Young's modulus set at 5 GPa and all other parameters constant (Figure 3E–H). As the Hamaker constant was increased from 0.5 to 2 aJ, the simulated measured height of the step became smaller (Figure 3E). By increasing the Hamaker constant, a larger magnitude (more negative) tip/sample attractive force was felt between the tip and surface. The increased attractive force between the tip and surface resulted in the tip being pulled deeper into the compliant surface, as can be seen from plotting the position of the tip with respect to the surface (Figure 3F). Despite being pulled deeper into the surface, the contact time between the tip and surface did not appreciably change, as can be seen from the position and time-resolved force plots (Figure 3F,G). While increases in Hamaker constant resulted in larger (more negative) attractive forces between the tip and surface at the beginning and end of each tapping event (Figure 3G), the total force per oscillation cycle was maintained by the feedback loop, which is a prerequisite to successful tracking of the surface topography. To compensate for the increased attractive force associated with each tapping event, the F_{max} increased with larger values of the Hamaker constant (Figure 3G). The larger F_{max} associated with increases in the Hamaker constant arose from the increased attractive force between the tip and sample pulling the probe deeper into the surface, which enlarged the force associated with the Hertzian term in eq 3. As a result, both F_{max} and F_{min} changed in magnitude linearly in response to the Hamaker constant; however, the sign of the forces was different (Figure 3H). Collectively, these simulations demonstrated that specific features of the time-resolved tip/sample tapping force are responsive to changes in the mechanical properties of the surface. Specifically, F_{min} linearly changed in response to increased adhesive force between the tip and surface as simulated by changing the Hamaker constant. These changes in F_{min} were independent of the Young's modulus under these simulation conditions. Despite the complication that F_{max} is dependent on both the Hamaker constant (linearly) and Young's modulus (power law), estimations of the rigidity (Young's modulus) of the surface can still be made because the contribution to F_{max} due to changes in the Hamaker constant can be estimated from F_{min}.

The Role of Set-Point on Time-Resolved Tip/Sample Force. While simulations indicated that the F_{max} and F_{min} can be useful indicators of the mechanical properties of surfaces, the impact of imaging conditions (such as set-point) on the observed time-resolved tip/surface force must be fully understood so that comparisons across samples can be easily made. To determine how the relative magnitude of F_{max} and F_{min} changed with varying the set-point ratio, experiments on the same TBLE bilayer patches supported on mica were performed (Figure 4). The temperature was maintained between 23 and 24 °C for these experiments to prevent any variations in the phase of the supported bilayer patch. The presence of exposed mica acts as an internal reference to study the relative values of tapping forces on the supported TBLE bilayer. Supported bilayers have a considerably lower elastic modulus compared to mica, so this system provides a surface with a soft region (supported bilayer) and hard region (mica). The set-point ratio had no discernible effect on the measured height of the supported bilayer patches (Figure 4A,B), as the mean distance between the height of the mica substrate (~0 nm) and the top of the supported bilayer (~3.6–3.9 nm) did not appreciably or systematically change as a function of set-point ratio. However, this observed supported bilayer height was smaller than would be expected for an uncompressed TBLE bilayer (~5 nm), indicating that the supported bilayer was compliant under the applied imaging force of the probe. As demonstrated in the

dx.doi.org/10.1021/la302705f | Langmuir 2012, 28, 13411–13422

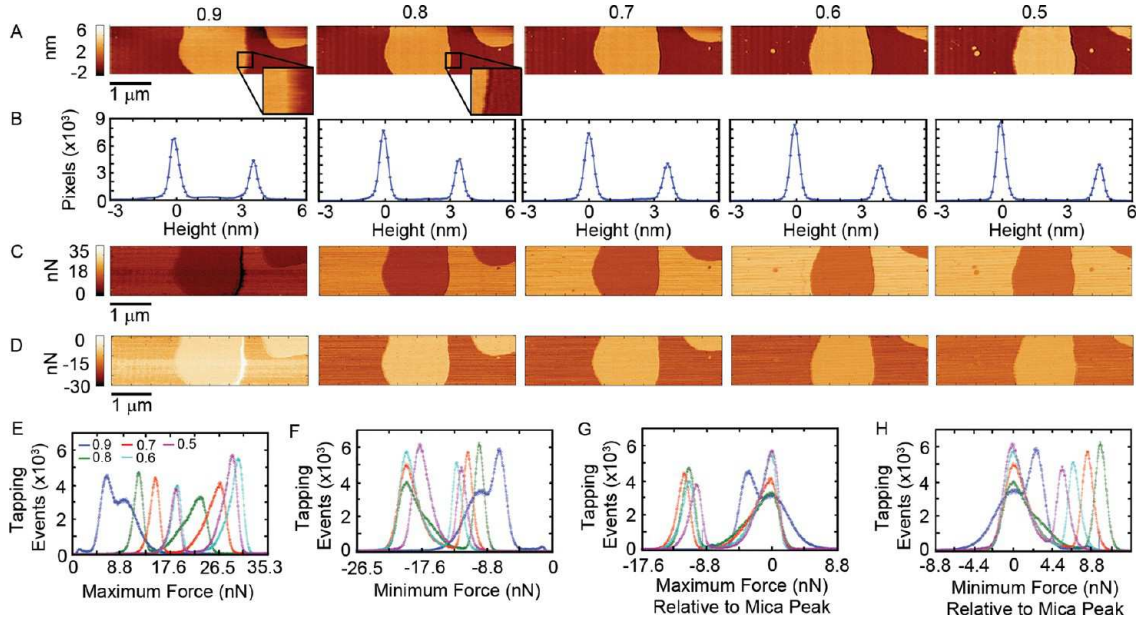

Figure 4. Effect of set-point ratio on the relative maximum and minimum tapping forces on mica and lipid bilayer patches. A series of fluid tapping mode AFM (A) topography images and (B) height histograms of the same TBLE lipid bilayer patch imaged with different set point ratios as indicated are presented. Insets in (A) demonstrate the tracking of the edge of the bilayer in the image. (C) Maximum tapping and (D) minimum tapping force images corresponding to the topography images obtained with different set point ratios are also presented. These maximum and minimum tapping force images were acquired by using the SPAM method. Raw histograms were constructed for (E) maximum forces measured from each individual tap during the imaging process, and then (F) histograms were aligned with respect to the average maximum tapping forces associated with imaging the exposed mica. As a result, the peak associated with maximum tapping forces on mica is centered around zero in the aligned histogram. Raw histograms were constructed for (G) minimum forces measured from each individual tap during the imaging process, and then (H) histograms were aligned with respect to the average minimum tapping forces associated with imaging the exposed mica. As a result, the peak associated with minimum tapping forces on mica is centered around zero in the aligned histogram.

simulations, the F_{max} associated with imaging regions of different rigidity decreased with decreasing elastic modulus; therefore, surface maps of the maximum tapping force can indicate regions of the surface with varying elastic modulus (Figure 4C). The magnitude of F_{max} is smaller in regions associated with the supported bilayer, indicating that the supported bilayer is softer than the mica, which is expected. Contrast was also observed in surface maps of F_{min} for the supported bilayer patch/mica system (Figure 4D), and this contrast between supported bilayer and mica can be attributed to adhesion to the tip.

While the measured height of the supported bilayer did not change as a function of set-point ratio, the magnitudes of F_{max} and F_{min} changed with decreasing set-point ratio (Figure 4E,F). For both F_{max} and F_{min}, histograms of the forces for each tapping event associated with obtaining the image are bimodal. The two peaks in the F_{max} and F_{min} histograms correspond to the mica and supported bilayer portions of the surface. For F_{max} the larger magnitude force is associated with mica. The larger magnitude (more negative) F_{min} is also associated with mica. As the set-point is lowered, the applied total force per tapping event to the surface increased, resulting in larger values of F_{max}, which is consistent with previously reported simulations and experiments (Figure 4E).[44] However, when the force histograms are normalized to F_{max} associated with mica, the relative value of F_{max} on the supported bilayer with respect to mica was maintained for set-point ratios of 0.5−0.8. The relative value of F_{max} associated with supported bilayer with respect to mica was smaller for an image captured with a set-point ratio of 0.9 because at this set-point the tip was barely tapping the surface, reducing the physical interaction between the tip and surface. This is further indicated by the decreased ability to properly track the edges of the supported bilayer with a set-point ratio of 0.9 in comparison to lower set-point ratios (Figure 4A insets). This indicates that once a certain set-point is reached, the relative tip/surface interactions associated with F_{max} on surfaces of varying elasticity remains constant. This observation makes comparisons between samples easier as long as an internal reference surface (such as mica) is present, simplifying calibration of such images with respect to relative surface properties. Once the set-point has been reduced below 0.9, the raw magnitude of F_{min} associated with mica does not appreciably change; however, F_{min} associated with the supported bilayer becomes larger in magnitude (Figure 4G). When the force histograms were normalized to F_{min} associated with mica (Figure 4H), the relative value of F_{min} on the supported bilayer with respect to mica systematically decreased as the set-point ratio was reduced from 0.8 to 0.5. This indicates that the relative values of F_{min} are dependent on the set-point ratio used, and care must be taken to maintain the same set-point ratio when using F_{min} values to compare between separate samples. Again, the relative values of F_{min} associated with supported bilayer and mica with a set-point ratio of 0.9 do not follow the pattern because the tip was barely tapping the surface, as is evidenced by the poor tracking on the edge of the supported bilayer compared to the deeper set-point ratios (Figure 4A insets).

Mechanical Properties of TBLE Supported Bilayers Change as a Function of Cholesterol Content. To determine if the time-resolved tip/sample tapping force could be used to detect physical changes in supported lipid bilayers associated with their composition, a series of experiments on

dx.doi.org/10.1021/la302705f | *Langmuir* 2012, 28, 13411−13422

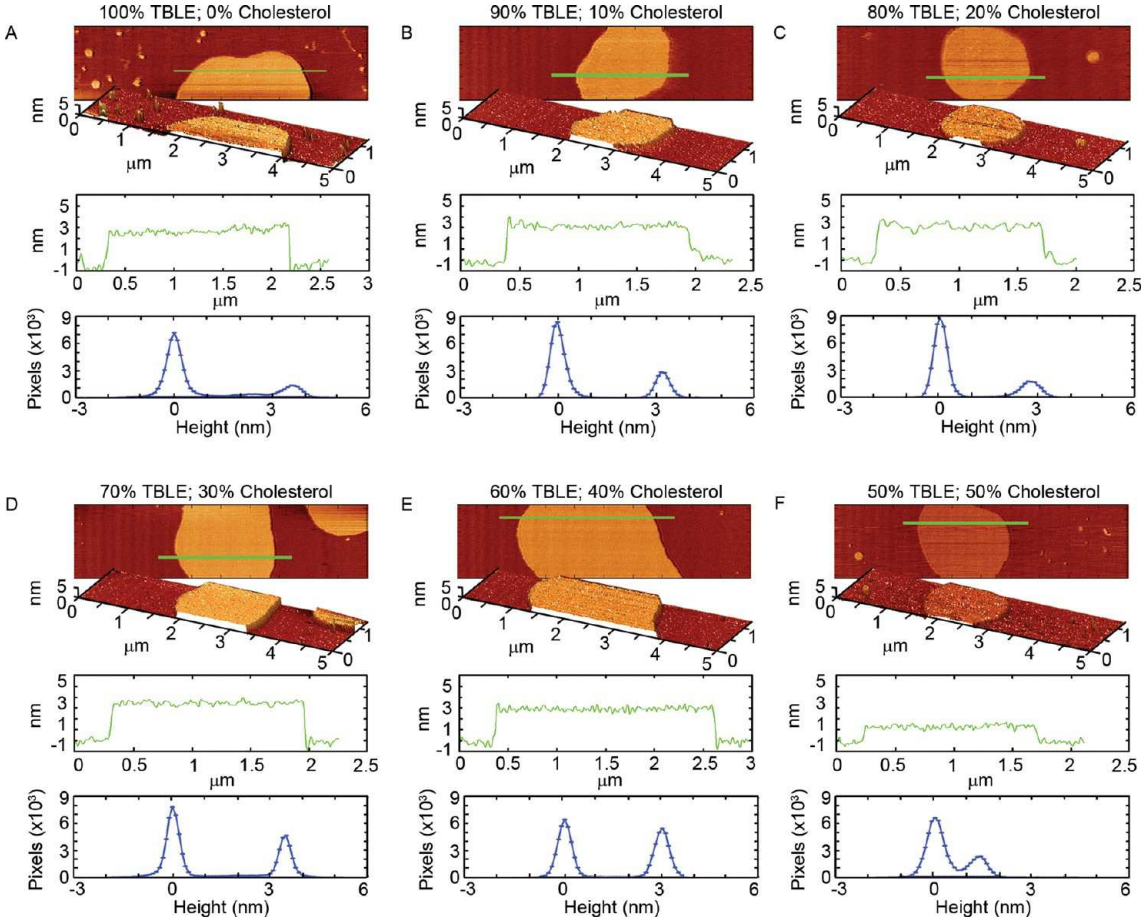

Figure 5. Effect of cholesterol content on the measured height of a TBLE bilayer. (A–E) A series of fluid tapping mode AFM images of TBLE bilayer patches enriched in cholesterol and supported on a mica surface imaged at the same free amplitude and set-point ratio. For each system, 2D and 3D height images are presented with a height profile taken from the image as indicated by the green line. Directly under each profile is a histogram of all pixels in the image. In these histograms, measurements associated with the mica substrate are centered around 0 nm.

supported TBLE bilayer patches on mica were performed. The supported TBLE bilayers were systematically enriched with exogenous cholesterol. Because of the TBLE being a complex mixture of lipid components, the cholesterol content was based on mass percentage. The samples used were (1) 100% TBLE, (2) 90% TBLE + 10% exogenous cholesterol, (3) 80% TBLE + 20% exogenous cholesterol, (4) 70% TBLE + 30% exogenous cholesterol, (5) 60% TBLE + 40% exogenous cholesterol, and (6) 50% TBLE + 50% exogenous cholesterol. This provides us with a simple system to determine the effectiveness of SPAM in measuring changes in physical properties of supported bilayers due to composition. Each of these samples was imaged between 23 and 24 °C. As this study requires cleaning the AFM fluid cell and cantilever after imaging each TBLE/cholesterol system, the knowledge gained on the effects of set-point ratio were necessary to facilitate comparison between samples. Based on the set-point ratio studies, a constant drive amplitude, free amplitude, and set-point ratio of 0.8 were used for all images. To further simplify comparison between samples, the same cantilever was used for all experiments. By using the same cantilever and imaging parameters, it is possible to compare forces across experiments because the total tip/sample force per oscillation cycle is given by

$$F_{\text{total}} \approx 0.5ka_0\frac{\Delta A}{A_0} \tag{11}$$

where k is the spring constant, a_0 is the drive amplitude, ΔA is the tapping amplitude, and A_0 is the free amplitude.[45] The forces associated with imaging the exposed mica can also be used as an internal reference to normalize small variations in the tip/sample force interaction, making it possible to compare relative shifts in the magnitude of tapping forces.[44]

At a given free amplitude and set-point ratio, the height of the supported bilayer patches with respect to the underlying mica substrate changed as a function of addition of cholesterol (Figure 5). Pure supported TBLE bilayers had a measured height of 3.6 nm (consistent with those observed for the set-point ratio experiments shown in Figure 4). As the exogenous cholesterol was increased from 0% to 20%, the measured height of the supported bilayer systematically decreased from 3.6 to 2.7 nm. At 30% exogenous cholesterol, the measured height of the supported bilayer increased to 3.5 nm. Adding more cholesterol to the supported bilayer resulted in mean height of the supported bilayer being 3.0 and 1.4 nm for 40% and 50% exogenous cholesterol, respectively. Based on simulations, changes in the Young's modulus or Hamaker constant associated with adding cholesterol to the supported bilayers could be associated with these observed changes in measured supported bilayer height. The greatly decreased measured height for 50% exogenous cholesterols was potentially caused by several factors. One possibility is that the supported bilayer approaching its cholesterol saturation point which can prevent

dx.doi.org/10.1021/la302705f | Langmuir 2012, 28, 13411–13422

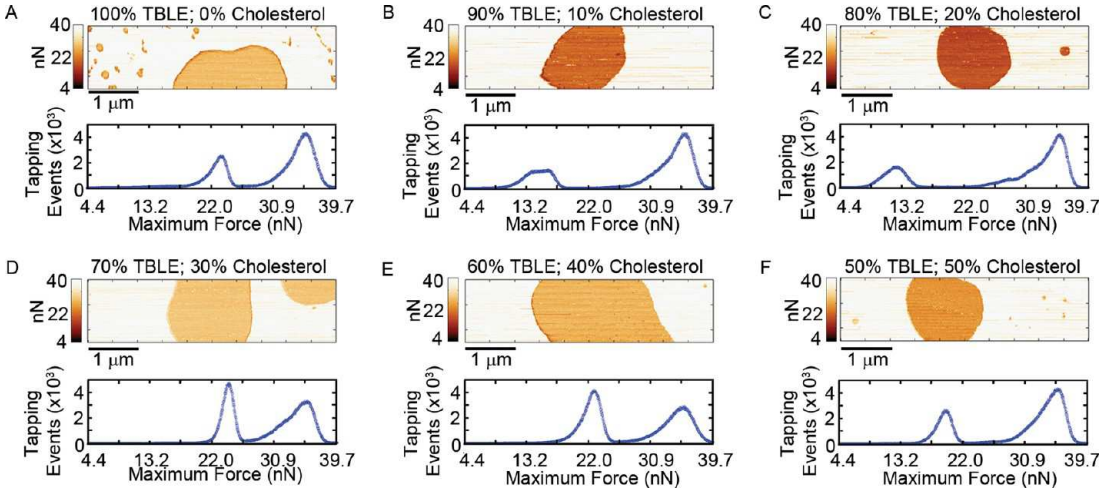

Figure 6. Reconstructed maximum tapping force images of TBLE + cholesterol bilayer patches supported on mica. F_{min} images associated with (A) 100% TBLE and 0% cholesterol, (B) 90% TBLE and 10% cholesterol, (C) 80% TBLE and 20% cholesterol, (D) 70% TBLE and 30% cholesterol, (E) 60% TBLE and 40% cholesterol, and (F) 50% TBLE and 50% cholesterol are presented. These images correspond to the height images presented in Figure 5. Histograms of the maximum tapping force associated with each image are provided directly below each image.

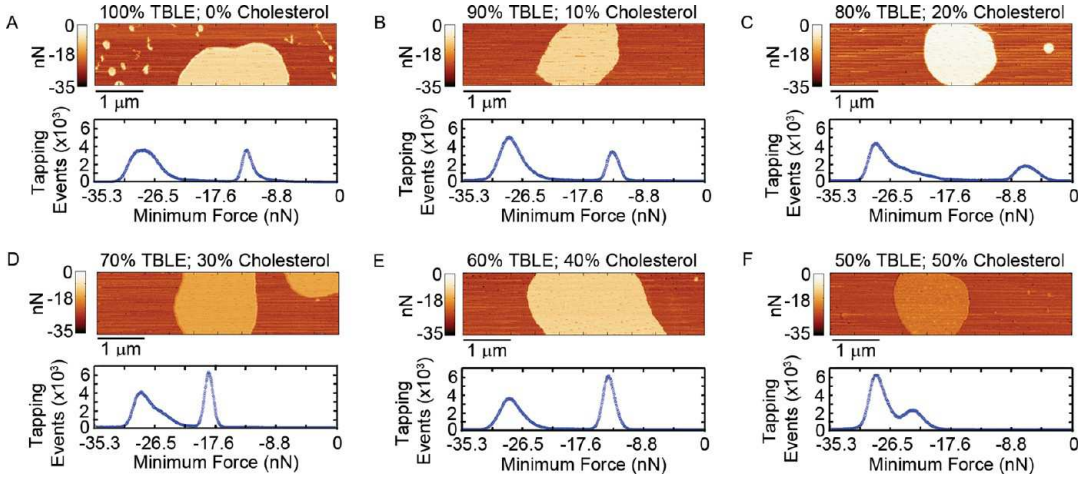

Figure 7. Reconstructed minimum tapping force images of TBLE + cholesterol bilayer patches supported on mica. F_{min} images associated with (A) 100% TBLE and 0% cholesterol, (B) 90% TBLE and 10% cholesterol, (C) 80% TBLE and 20% cholesterol, (D) 70% TBLE and 30% cholesterol, (E) 60% TBLE and 40% cholesterol, and (F) 50% TBLE and 50% cholesterol are presented. These images correspond to the height images presented in Figure 5. Histograms of the minimum tapping force associated with each image are provided directly below each image.

efficient lipid packing into ordered bilayers.[19] Several groups have reported that at cholesterol concentrations equal to and greater than 50% that the cholesterol is insoluble in the bilayer and precipitation can occur.[27,46] Therefore, the increased compressibility may be attributed to the inability of the lipid to completely incorporate the shorter cholesterol molecules. The shorter cholesterol molecules within the bilayer, which are known to have a length of about 2 nm,[47,48] may also be contributing to the shorter observed supported bilayer patches. The thickness of bilayers does change due to the addition of exogenous cholesterol, with the bilayer thickness increasing initially with additional cholesterol before reaching a maximum thickness and decreasing.[29] Another possibility is a cholesterol-induced phase change in the supported lipid bilayer.

To determine the dominant contributor to the observed supported bilayer heights as a function of cholesterol content, the F_{max} and F_{min} for every tapping event were reconstructed using the SPAM method and used to construct F_{max} and F_{min} surface maps (Figures 6 and 7) that correspond directly to the topography images (Figure 5). While F_{max} is a measure of the surfaces local Young's modulus, F_{min} is related to the force required to break contact between the tip and surface, i.e. adhesion, and can be associated with local changes in surface free energy, as we have demonstrated with simulations. There is a bimodal distribution in histograms of F_{max} and F_{min} associated with the supported TBLE bilayer and mica images. For F_{max}, the smaller positive force is associated with the supported lipid bilayers (which was variable for the different supported bilayer systems), indicating that the supported bilayers have a lower elastic modulus than the mica substrate ($F_{max} \sim 35$ nN). The population of the smaller magnitude F_{min} is associated with the supported lipid bilayers, indicating that the tip/supported bilayer interaction (which had variable F_{min} values depending on cholesterol content) has a smaller surface free energy compared to the tip/mica substrate interaction ($F_{min} \sim -28.5$ nN). The shift in the observed magnitudes of F_{max} and F_{min} associated with supported bilayers with respect to the mica surface indicates that the addition of cholesterol altered the

dx.doi.org/10.1021/la302705f | Langmuir 2012, 28, 13411−13422

mechanical properties of the supported bilayers (histograms in Figures 6 and 7).

As the cantilever (i.e., same spring constant and mass) and imaging parameters (i.e., drive amplitude, free amplitude, and set-point ratio) were maintained in all experiments, features of the time-resolved tip/sample tapping forces on the different supported bilayer systems can be directly compared (Figure 8).

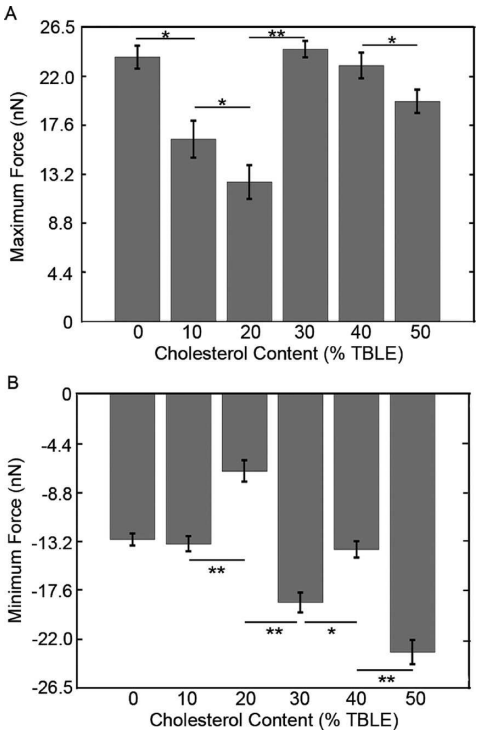

Figure 8. Average values of the (A) maximum and (B) minimum tapping force on TBLE lipid bilayer patches as a function of exogenous cholesterol content. The average values are taken from all tapping events occurring on bilayer patches, and the error bars represent the standard deviation. ∗ indicates $p < 0.05$; ∗∗ indicates $p < 0.01$ based on a simple t test.

A smaller F_{max} associated with imaging the supported bilayer correlates with a smaller elastic modulus after taking into account any contributions due to any increased attractive interaction, which can be estimated based on F_{min}. Initially, there was a decrease in F_{max} as the cholesterol content of the supported bilayer is increased from 0% to 20% (Figure 8A). The change in F_{max} associated with increasing the exogenous cholesterol content of the supported bilayers from 0% to 10% and 10% to 20% was significant ($p < 0.05$). This was followed by a dramatic increase in F_{max} when 30% exogenous cholesterol was added to the supported bilayers ($p < 0.01$ when comparing 20% exogenous cholesterol to 30% exogenous cholesterol). While no significant change was observed in F_{max} when the exogenous cholesterol was increased from 30% to 40%, another significant ($p < 0.05$) decrease in F_{max} was observed when more exogenous cholesterol was added (up to 50%). This bimodal pattern indicates an initial decrease in Young's modulus of the supported bilayer with the addition of cholesterol, followed by a sharp increase in the Young's modulus, followed with another decrease. Interestingly, the observed heights of the supported bilayers with 0% to 40% exogenous cholesterol correspond well with the magnitude of the associated magnitude of F_{max}. That is, the supported bilayers with the smallest values of F_{max}, which should be the most easily compressed based on associated relative value of Young's modulus, have smaller observed heights. This relationship did not hold true for the 50% cholesterol supported bilayer, which again may be due partially to the supported bilayer being near its cholesterol saturation concentration.[19] The bimodal pattern of the values of F_{max} associated with the supported bilayer as a function of cholesterol content is intriguingly similar to the pattern observed by Yip et al. for membrane fluidity on the same system using fluorescence DPH (diphenylhexatriene) anisotropy.[26] In that study, it was shown that the membrane fluidity decreased with exogenous addition of cholesterol to TBLE up to 20%, had a maximum lateral fluidity at 30% exogenous cholesterol, and decreased again with the further addition of cholesterol to the TBLE bilayer.[26] A caveat of this comparison is that these measurements were performed on lipid vesicles rather than the supported bilayer systems used here. The mica substrate can influence the fluidity of the supported lipid bilayer, causing it to be different than that observed in the lipid vesicle system. However, this still hints at the interesting possibility that there is a relationship between lateral fluidity and vertical compressibility of lipid membranes in which the larger the lateral fluidity of the membrane the larger the Young's modulus. Such a scenario would be advantageous for biological membranes that need to balance lateral mobility within the membrane to maintain structural integrity of the membrane as a whole. It has been reported that molecules, such as cholesterol, which lie parallel to a lipid chain will experience only slight perturbations if pressure is applied in the vertical direction; however, the horizontal compressibility can be much greater,[49] which may partially explain the potential relationship between vertical compressibility and lateral fluidity of a lipid bilayer. Similar increases in bilayer compression perpendicular to the membrane plane have been observed in other simpler bilayer systems, but the exact changes in elasticity due to addition of cholesterol are dependent on the nature of the phospholipids.[27] Another potential factor causing the observed changes in relative Young's modulus with the addition of exogenous cholesterol could be due to changes in the phase of the supported bilayer, as cholesterol has been shown to induce transitions from the liquid disordered to the liquid ordered phase in POPC bilayer vesicles.[50] Such cholesterol-induced phase transitions have been shown to have biological relevance as the membrane structure associated with the lipid phase appears to be the determining factor in the pore-forming activity of the polyene antibioitic nystatin on POPC/cholesterol vesicles.[51]

F_{min} provides information about the adhesive force between the AFM probe and supported bilayer surface. That is, the larger the magnitude of F_{min}, the more adhesive the surface is to the AFM tip. F_{min} as a function of cholesterol content did not demonstrate the same pattern as seen in F_{max} (Figure 8B) or the bilayer fluidity data from Yip et al.[26] The adhesion between the bilayer and tip did not appreciably change with the addition of 10% exogenous cholesterol. At 20% exogenous cholesterol, the adhesive force between the tip and bilayer decreased significantly ($p < 0.01$), but the adhesion became much stronger with the addition of 30% cholesterol ($p < 0.01$). The adhesive force at 40% cholesterol was similar to that of a pure TBLE bilayer and one containing 10% cholesterol; however, this represented a significant decrease in the adhesive force when comparing samples with 30% exogenous cholesterol. There is an interesting feature in which the adhesive force is

dx.doi.org/10.1021/la302705f | Langmuir 2012, 28, 13411−13422

largest when the bilayer contains 50% exogenous cholesterol, and this increase in adhesive force was significant ($p < 0.01$). As simulations have demonstrated that large adhesive forces can result in an increased compression of soft surfaces, this large increase in adhesion could also contribute to the lower observed height as measured by AFM. This could further explain why the measured height of the 50% exogenous cholesterol bilayer was an outlier to the observed relationship between F_{max} and measured bilayer height. A potential complication of this type of analysis is the potential of a lipid layer forming on the AFM tip. Based on the topography images, there was no evidence that this occurred in any of the presented experiments. Precautions were used to avoid this complicating factor. Between experiments, the cantilever and fluid cell were cleaned to prevent any cross-contamination. If a lipid bilayer would have formed on the AFM tip, this would be a similar situation to tapping a double bilayer. On the basis of published results from Xu et al. of contrast associated with higher harmonic frequencies in tapping mode AFM experiments on supported purple membranes that were one or two layers thick,[52] we suspect that the associated tapping forces would be altered by a bilayer forming on the surface of the tip, as double bilayers are more compressible than single bilayers.

Mechanical Properties of Lipid Rafts Are Distinguishable from the Rest of a Supported Lipid Bilayer. When heating supported TBLE bilayers with 30% exogenous cholesterol above 35 °C, the mean height of the bilayer patch above the mica surface was reduced to ∼2.4 nm (Figure 9A). Furthermore, small lipid raft domains formed within the supported bilayer patch (Figure 9B). These lipid domains were ∼0.7−1.2 nm lower in height compared to the rest of the supported bilayer, and the rafts (based on topography) ranged in diameter from ∼75−250 nm. These supported bilayers with rafts were imaged at 35 °C, and the forces associated with each tapping event were reconstructed using SPAM to obtain F_{max} and F_{min} images (Figure 9C,D). It should be noted that a different cantilever was used in this experiment, resulting in different observed magnitudes of tapping forces compared to the previously described cholesterol content experiments. Contrast in the F_{max} and F_{min} associated with the lipid raft domains was observed, and histograms of F_{max} and F_{min} were sorted based on the associated topography image (Figure 9C,D). The lipid raft domains were associated with an increase in F_{max} compared to the rest of the supported TBLE bilayer. The F_{min} associated with the lipid raft domains also increased in magnitude relative to the rest of the supported bilayer. While the change in F_{max} may be partially due to an increased rigidity of the raft domains, the relative shifts associated with F_{max} and F_{min} were comparable, which indicates that the changes in the adhesive properties of the supported bilayer most likely is the dominant factor in the observed tapping forces (both F_{max} and F_{min}). The reduced height associated with the lipid raft domains would also be consistent with the decreased height differences associated with large adhesive forces. Importantly, these experiments demonstrate the ability of SPAM to distinguish mechanical properties with lateral resolution on the order of 75−250 nm. Similar to obtaining topography images with AFM, the lateral resolution associated with SPAM appears to be limited by the size of the tip and the contact area between the tip and surface.

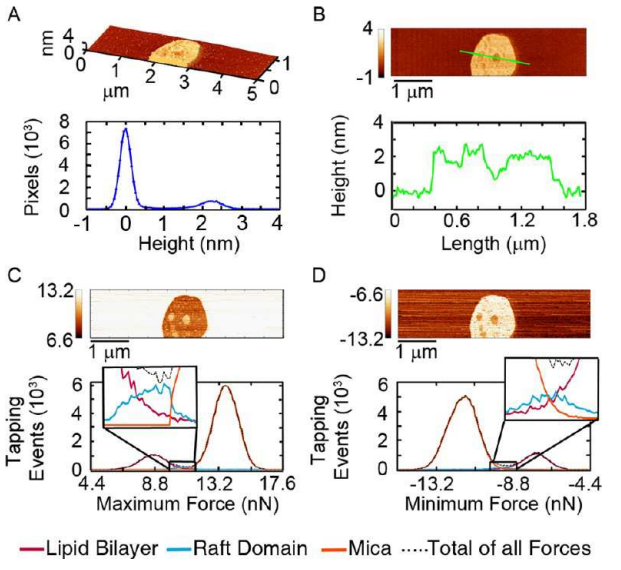

Figure 9. Lipid raft domains can form in these systems at elevated temperatures. (A) An AFM topography image and height histogram of a supported lipid bilayer (70% TBLE and 30% cholesterol) taken at 35 °C demonstrates the formation of lipid domains. (B) The green line in the image corresponds to the height profile that demonstrates that the lipid raft domains were ∼0.7−1.2 nm lower in height and had diameters of ∼75−250 nm . Reconstructed, spatially resolved images and corresponding histograms of (C) F_{max} and (D) F_{min} are shown. The forces associated with different regions of the surfaces were sorted in the histograms based on topography. The insets magnify the regions of the histogram associated with the lipid raft domains.

CONCLUSIONS

An important direction in the field of scanning probe techniques is the further development of methods to capture topographical and mechanical information about surfaces simultaneously. Reconstruction of the time-resolved tip/sample tapping force during standard operation of tapping mode AFM is one attractive method for achieving this goal, and several techniques have been developed to accomplish the recovery of these forces.[2,6−14] Presented simulations and experimental results demonstrated that the maximum and minimum observed tapping forces for tapping mode AFM operation in fluids can be related to material properties of surfaces such as Young's modulus and surface free energy between the tip and surface. The reconstructed tip/sample force interactions can provide insight into the mechanical properties of biologically relevant surfaces with nanoscale spatial resolution. The applicability of the SPAM technique, which enables the reconstruction of tapping forces from the deflection signal of a TMAFM experiment, to investigate the mechanical changes induced in supported lipid bilayer patches by the addition of exogenous cholesterol was demonstrated. In this particular study, maximum tapping forces provided evidence for a link between vertical compressibility and lateral fluidity of a membrane, as was demonstrated with supported TBLE bilayers containing various amounts of exogenous cholesterol. In addition, minimum tapping forces provided information about adhesive properties of the supported lipid bilayer to the AFM probe. These studies on supported bilayers enriched in cholesterol demonstrate that the SPAM technique is sensitive to the composition of the lipid system, and this technique may prove valuable in mapping relative mechancial properties of supported bilayers of other compositions. To facilitate comparison between samples, it is imperative to hold

several key parameters constant, such as drive amplitude, free amplitude, and set-point ratio. Many of these issues are simplified by using the same cantilever for all experiments. Importantly, all of these experiments were performed under physiologically relevant buffer conditions, which make this technique particularly applicable to the study of biologically relevant surfaces.

■ ASSOCIATED CONTENT

Supporting Information

Supplementary figure of the model used for simulations. This material is available free of charge via the Internet at http://pubs.acs.org.

■ AUTHOR INFORMATION

Corresponding Author

*E-mail: justin.legleiter@mail.wvu.edu.

Notes

The authors declare no competing financial interest.

■ ACKNOWLEDGMENTS

This work was supported by the Brodie Entrepreneurial and Development Fund and the National Science Foundation (NSF#CMMI1054211). N.S.-K. was supported by a graduate fellowship from WVnano (NSF Cooperative Agreement 1003907).

■ REFERENCES

(1) Li, J. K.; Sullan, R. M. A.; Zou, S. Atomic force microscopy force mapping in the study of supported lipid bilayers. *Langmuir* **2011**, *27*, 1308−1313.

(2) Legleiter, J.; Park, M.; Cusick, B.; Kowalewski, T. Scanning probe acceleration microscopy (SPAM) in fluids: Mapping mechanical properties of surfaces at the nanoscale. *Proc. Natl. Acad. Sci. U. S. A.* **2006**, *103*, 4813−4818.

(3) Garcia, R.; Perez, R. Dynamic atomic force microscopy methods. *Surf. Sci. Rep.* **2002**, *47*, 197−301.

(4) Zhong, Q.; Inniss, D.; Kjoller, K.; Elings, V. B. Fractured polymer/silica fiber surface studied by tapping mode atomic force microscopy. *Surf. Sci.* **1993**, *290*, 688−692.

(5) Stark, M.; Stark, R. W.; Heckl, W. M.; Guckenberger, R. Inverting dynamic force microscopy: From signals to time-resolved interaction forces. *Proc. Natl. Acad. Sci. U. S. A.* **2002**, *99*, 8473−8478.

(6) Balantekin, M.; Onaran, A. G.; Degertekin, F. L. Quantitative mechanical characterization of materials at the nanoscale through direct measurement of time-resolved tip-sample interaction forces. *Nanotechnology* **2008**, *19*, 085704.

(7) Garcia, R.; Herruzo, E. T. The emergence of multifrequency force microscopy. *Nat. Nanotechnol.* **2012**, *7*, 217−226.

(8) Sahin, O. Harnessing bifurcations in tapping-mode atomic force microscopy to calibrate time-varying tip-sample force measurements. *Rev. Sci. Instrum.* **2007**. *78* (10).

(9) Sahin, O. Time-varying tip-sample force measurements and steady-state dynamics in tapping-mode atomic force microscopy. *Phys. Rev. B* **2008**. *77* (11).

(10) Sahin, O.; Erina, N. High-resolution and large dynamic range nanomechanical mapping in tapping-mode atomic force microscopy. *Nanotechnology* **2008**. *19* (44).

(11) Sahin, O.; Magonov, S.; Su, C.; Quate, C. F.; Solgaard, O. An atomic force microscope tip designed to measure time-varying nanomechanical forces. *Nat. Nanotechnol.* **2007**, *2* (8), 507−514.

(12) Sarioglu, A. F.; Magonov, S.; Solgaard, O. Tapping-mode force spectroscopy using cantilevers with interferometric high-bandwidth force sensors. *Appl. Phys. Lett.* **2012**, *100*, 053109.

(13) Sarioglu, A. F.; Solgaard, O. Cantilevers with integrated sensor for time-resolved force measurement in tapping-mode atomic force microscopy. *Appl. Phys. Lett.* **2008**. *93* (2).

(14) Sarioglu, A. F.; Solgaard, O. Modeling, design, and analysis of interferometric cantilevers for time-resolved force measurements in tapping-mode atomic force microscopy. *J. Appl. Phys.* **2011**, *109*, 064316.

(15) Espinosa, G.; López-Montero, I.; Monroy, F.; Langevin, D. Shear rheology of lipid monolayers and insights on membrane fluidity. *Proc. Natl. Acad. Sci. U. S. A.* **2011**, *108*, 6008−6013.

(16) Singer, S. J.; Nicolson, G. L. Fluid mosaic model of structure of cell-membranes. *Science* **1972**, *175*, 720−731.

(17) van Meer, G. V. D. R.; Feigenson, G. W. Membrane lipids: where they are and how they behave. *Nat. Rev. Mol. Cell Biol.* **2008**, *9*, 112−124.

(18) Evans, E.; Needham, D. Physical properties of surfactant bilayer membranes: thermal transitions, elasticity, rigidity, cohesion and colloidal interactions. *J. Phys. Chem.* **1987**, *91*, 4219−4228.

(19) Needham, D.; Nunn, R. S. Elastic deformation and failure of lipid bilayer membranes containing cholesterol. *Biophys. J.* **1990**, *58*, 997−1009.

(20) Pan, J.; Mills, T. T.; Tristram-Nagle, S.; Nagle, J. F. Cholesterol perturbs lipid bilayers nonuniversally. *Phys. Rev. Lett.* **2008**, *100*, 198103.

(21) Mukherjee, S.; Maxfield, F. R. Membrane domains. *Annu. Rev. Cell Dev. Biol.* **2004**, *20*, 839−866.

(22) Simons, K.; Vaz, W. L. C. Model systems, lipid rafts, and cell membranes. *Annu. Rev. Biophys. Biomol. Struct.* **2004**, *33*, 269−295.

(23) Goldstein, J. L.; Brown, M. S. Molecular medicine - The cholesterol quartet. *Science* **2001**, *292*, 1310−1312.

(24) Maxfield, F. R.; Tabas, I. Role of cholesterol and lipid organization in disease. *Nature* **2005**, *438*, 612−621.

(25) Asakawa, H.; Fukuma, T. The molecular-scale arrangement and mechanical strength of phospholipid/cholesterol mixed bilayers investigated by frequency modulation atomic force microscopy in liquid. *Nanotechnology* **2009**, *20*, 264008.

(26) Yip, C. M.; Elton, E. A.; Darabie, A. A.; Morrison, M. R.; McLaurin, J. Cholesterol, a modulator of membrane-associated ab-fibrillogenesis and neurotoxicity. *J. Mol. Biol.* **2001**, *311* (4), 723−734.

(27) Hianik, T.; Haburcak, M.; Lohner, K.; Prenner, E.; Paltauf, F.; Hermetter, A. Compressibility and density of lipid bilayers composed of polyunsaturated phospholipids and cholesterol. *Colloids Surf., A* **1998**, *139*, 189−197.

(28) Byfield, F. J.; Aranda-Espinoza, H.; Romanenko, V. G.; Rothblat, G. H.; Levitan, I. Cholesterol depletion increases membrane stiffness of aortic endothelial cells. *Biophys. J.* **2004**, *87*, 3336−3343.

(29) Hung, W.-C.; Lee, M.-T.; Chen, F.-Y.; Huang, H. W. The condensing effect of cholesterol in lipid bilayers. *Biophys. J.* **2007**, *92*, 3960−3967.

(30) Legleiter, J.; Fryer, J. D.; Holtzman, D. M.; Kowalewski, T. The modulating effect of mechanical changes in lipid bilayers caused by apoe-containing lipoproteins on Aβ induced membrane disruption. *ACS Chem. Neurosci.* **2011**, *2*, 588−599.

(31) Pifer, P. M.; Yates, E. A.; Legleiter, J. Point mutations in Aβ Result in the formation of distinct polymorphic aggregates in the presence of lipid bilayers. *PLoS One* **2011**, *6* (1), e16248.

(32) Tsinman, O.; Tsinman, K.; Sun, N.; Avdeef, A. Physicochemical selectivity of the BBB microenvironment governing passive diffusion—matching with a porcine brain lipid extract artificial membrane permeability model. *Pharm. Res.* **2011**, *28*, 337−363.

(33) Burnham, N. A.; Behrend, O. P.; Oulevey, F.; Gremaud, G.; Gallo, P.-J.; Gourdon, D.; Dupas, E.; Kulik, A. J.; Pollock, H. M.; Briggs, G. A. D. How does a tip tap? *Nanotechnology* **1997**, *8* (2), 67−75.

(34) Kuhle, A.; Sorensen, A. H.; Bohr, J. Role of attractive forces in tapping tip force microscopy. *J. Appl. Phys.* **1997**, *81*, 6562−6569.

(35) Salapaka, M. V.; Chen, D. J.; Cleveland, J. P. Linearity of amplitude and phase in tapping-mode atomic force microscopy. *Phys. Rev. B* **2000**, *61* (2), 1106.

(36) Song, Y. X.; Bhushan, B. Atomic force microscopy dynamic modes: modeling and applications. *J. Phys.: Condens. Matter* **2008**, *20*, 22.
(37) Basak, S.; Raman, A. Dynamics of tapping mode atomic force microscopy in liquids: Theory and experiments. *Appl. Phys. Lett.* **2007**, *91* (6), 064107.
(38) Xu, X.; Carrasco, C.; de Pablo, P. J.; Gomez-Herrero, J.; Raman, A. Unmasking imaging forces on soft biological samples in liquids when using dynamic atomic force microscopy: A case study on viral capsids. *Biophys. J.* **2008**, *95* (5), 2520−2528.
(39) Israelachvili, J. *Intermolecular & Surface Forces*; Academic: London, 1992; p 450.
(40) Derjaguin, B. V.; Muller, V. M.; Toporov, Y. P. Effect of contact deformations on the adhesion of particles. *J. Colloid Interface Sci.* **1975**, *53* (2), 314−326.
(41) Legleiter, J.; Kowalewski, T. Insights into fluid tapping-mode atomic force microscopy provided by numerical simulations. *Appl. Phys. Lett.* **2005**, *87* (16), 163120−3.
(42) Putman, C. A. J.; Van der Werf, K. O.; De Grooth, B. G.; Van Hulst, N. F.; Greve, J. Tapping mode atomic force microscopy in liquid. *Appl. Phys. Lett.* **1994**, *64* (18), 2454−2456.
(43) Hutter, J. L.; Bechhoefer, J. Calibration of atomic-force microscope tips. *Rev. Sci. Instrum.* **1993**, *64*, 1868−1873.
(44) Kumar, B.; Pifer, P. M.; Giovengo, A.; Legleiter, J. The effect of set point ratio and surface Young's modulus on maximum tapping forces in fluid tapping mode atomic force microscopy. *J. Appl. Phys.* **2010**, *107*, 044508.
(45) Kowalewski, T.; Legleiter, J. Imaging stability and average tip-sample force in tapping mode atomic force microscopy. *J. Appl. Phys.* **2006**, *99*, 064903.
(46) Ibarguren, M.; Alonso, A.; Tenchov, B. G.; Goñi, F. M. Quantitation of cholesterol incorporation into extruded lipid bilayers. *Biochim. Biophys. Acta, Biomembr.* **2010**, *1798*, 1735−1738.
(47) Craven, B. M. Crystal structure of cholesterol monohydrate. *Nature* **1976**, *260*, 727−729.
(48) Sankaram, M. B.; Thompson, T. E. Modulation of phospholipid acyl chain order by cholesterol. A solid-state deuterium nuclear magnetic resonance study. *Biochemistry* **1990**, *29*, 10676−10684.
(49) Scarlata, S. F. Compression of lipid membranes as observed at varying membrane positions. *Biophys. J.* **1991**, *60*, 334−340.
(50) Silva, L.; Coutinho, A.; Fedorov, A.; Prieto, M. Competitive binding of cholesterol and ergosterol to the polyene antibiotic nystatin. A fluorescence study. *Biophys. J.* **2006**, *90* (10), 3625−3631.
(51) Gonzalez-Damian, J.; Ortega-Blake, I. Effect of membrane structure on the action of polyenes II: nystatin activity along the phase diagram of ergosterol- and cholesterol-containing POPC membranes. *J. Membr. Biol.* **2010**, *237* (1), 41−49.
(52) Xu, X.; Melcher, J.; Basak, S.; Reifenberger, R.; Raman, A. Compositional contrast of biological materials in liquids using the momentary excitation of higher eigenmodes in dynamic atomic force microscopy. *Phys. Rev. B* **2009**, *102* (6), 060801−4.

Supplemental Material for:

Mapping the mechanical properties of cholesterol-containing supported lipid bilayers with nanoscale spatial resolution

Nicole Shamitko-Klingensmith[1,2], *Kelley M. Molchanoff*[2], *Kathleen A. Burke*[1], *George J. Magnone*[1], *Justin Legleiter*[1,2,3,*]

[1]The C. Eugene Bennett Department of Chemistry; [2]WVnano SAFE; [3]the Center for Neurosciences, West Virginia University, Morgantown, WV 26505, USA.

TITLE RUNNING HEAD. Mapping the mechanical properties of surfaces in solution.

Address correspondence to justin.legleiter@mail.wvu.edu.

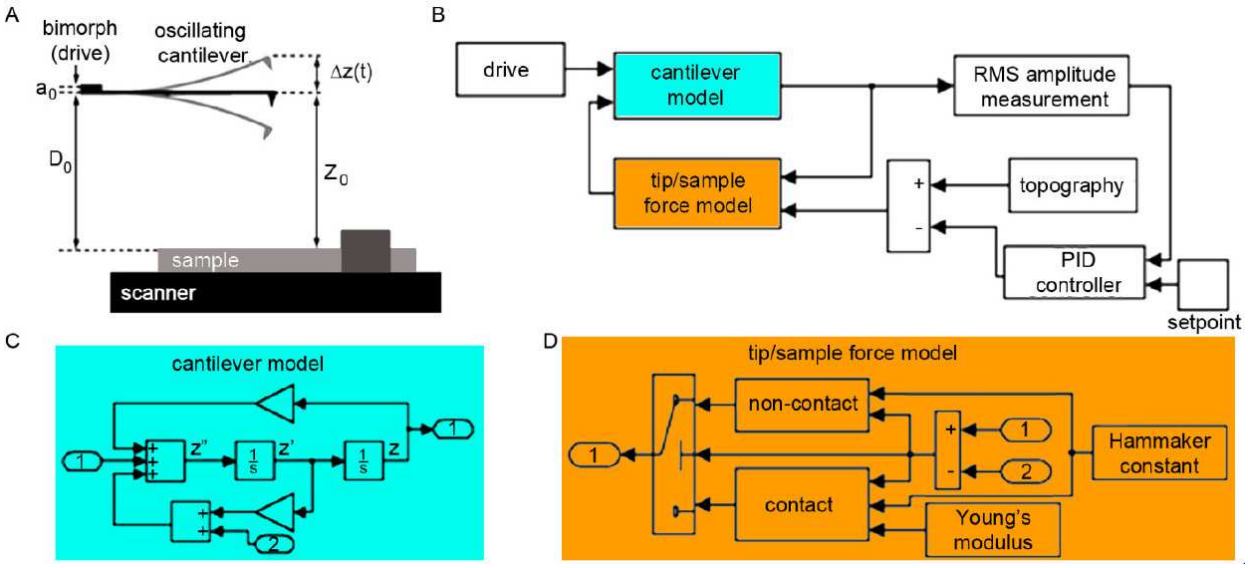

Supplemental Figure 1. Numerical simulation of the entire process of obtaining an AFM image were performed. (A) Schematic illustration of a tapping mode AFM experimental set-up illustrating several parameters used to model cantilever dynamics. (B) The SIMULINK model used for performing numerical simulations. Key features of the model include the cantilever drive, cantilever model (shown in further detail in (C)), the tip/sample force model which contains the ability to change the Young's modulus and the Hamaker constant (shown in further detail in (D)), the amplitude measurement, the topography model, feedback loop equipped with a PID controller, and the set point parameter.